The Astrophysical Journal, 801:30 (5pp), 2015 March 1 doi:10.1088/0004-637X/801/1/30

OCCURRENCE OF HIGH-SPEED SOLAR WIND STREAMS OVER THE GRAND MODERN MAXIMUM

K. Mursula[1], R. Lukianova[2,3], and L. Holappa[1]
[1] ReSoLVE Centre of Excellence, Department of Physics, University of Oulu, Finland; kalevi.mursula@oulu.fi
[2] Geophysical Center of Russian Academy of Science, Moscow, Russia
[3] Space Research Institute, Moscow, Russia
Received 2014 July 30; accepted 2014 December 23; published 2015 February 27

ABSTRACT

In the declining phase of the solar cycle (SC), when the new-polarity fields of the solar poles are strengthened by the transport of same-signed magnetic flux from lower latitudes, the polar coronal holes expand and form non-axisymmetric extensions toward the solar equator. These extensions enhance the occurrence of high-speed solar wind (SW) streams (HSS) and related co-rotating interaction regions in the low-latitude heliosphere, and cause moderate, recurrent geomagnetic activity (GA) in the near-Earth space. Here, using a novel definition of GA at high (polar cap) latitudes and the longest record of magnetic observations at a polar cap station, we calculate the annually averaged SW speeds as proxies for the effective annual occurrence of HSS over the whole Grand Modern Maximum (GMM) from 1920s onward. We find that a period of high annual speeds (frequent occurrence of HSS) occurs in the declining phase of each of SCs 16–23. For most cycles the HSS activity clearly reaches a maximum in one year, suggesting that typically only one strong activation leading to a coronal hole extension is responsible for the HSS maximum. We find that the most persistent HSS activity occurred in the declining phase of SC 18. This suggests that cycle 19, which marks the sunspot maximum period of the GMM, was preceded by exceptionally strong polar fields during the previous sunspot minimum. This gives interesting support for the validity of solar dynamo theory during this dramatic period of solar magnetism.

Key words: solar-terrestrial relations – solar wind – Sun: activity – Sun: magnetic fields

1. INTRODUCTION

Properties of the solar wind (SW), the tenuous plasma emanating from the solar corona, have been directly monitored since the early 1960s, soon after the start of the space age. Figure 1(a) shows the annual means of the SW speed at Earth's orbit in 1964–2010, measured by a number of Earth-orbiting satellites and interplanetary probes collected in the NASA/NSSDC OMNI-2 database. One can see that SW speed depicts a cyclic variation, with maxima in the declining phase of the solar cycle (SC), when the polar coronal holes extend equatorward and emit high-speed SW streams (HSS) at sufficiently low latitudes to be detected at the Earth (Krieger et al. 1973; Bame et al. 1976; Kojima & Kakinuma 1990; Rickett & Coles 1991; Mursula & Zieger 1996).

It is known that the Sun experienced a period of exceptionally high sunspot activity during the 20th century (Solanki et al. 2004; Abreu et al. 2008), now termed the Grand Modern Maximum (GMM) of solar activity. Recent observations of declining sunspot magnetic field strengths (Penn & Livingston 2006; Livingston & Penn 2009), vanishing of small sunspots (Lefèvre & Clette 2011), and the weakness of the ongoing cycle 24 suggest that the GMM has reached its end. Because the maximum of the GMM was already reached during cycle 19 in the late 1950s, direct SW observations only exist from the declining phase of the GMM. Moreover, since systematic measurements of the solar global magnetic field started only in the 1970s, no direct information on solar polar fields exists from the ascending phase or the maximum of the GMM.

Geomagnetic activity (GA), i.e., the short-term variability of Earth's magnetic field, is driven by the SW and the interplanetary magnetic field (IMF). Figure 1(b) depicts the annual means of one of the most commonly used measures of GA, the aa index, since the 1920s (Mayaud 1972). The aa index depicts a somewhat different SC variation from the SW speed. For cycles 20 and 23, the aa index and SW speed have maxima in the same years, but for cycles 21 and 22 the cycle maximum of the aa index is earlier. Also, the relative heights of the four SC maxima are different in GA and in SW speed. These differences between SW speed and the aa index are due to the fact that not only high-speed streams but also coronal mass ejections (CMEs) are important SW structures driving GA at mid-latitudes, which is monitored through the aa index. However, since HSSs and CMEs have different SC occurrences, they have different relative contributions to GA over the SC (Richardson et al. 2002; Holappa et al. 2014). While high-speed streams reach maximum in the declining phase, the CMEs follow the sunspot cycle fairly reliably and are therefore more common around sunspot maxima.

The dependence of GA on SW speed is most direct in the auroral region (Finch et al. 2008), where strong horizontal currents called the auroral electrojets flow in the ionosphere, the ionized layer of the upper atmosphere. During magnetospheric substorms, whose occurrence reaches maximum in the years of persistent high-speed SW streams (Tanskanen et al. 2005), the westward auroral electrojet (WEJ) is extended in local time (LT) and enhanced in intensity, especially in the evening to pre-midnight sector, causing a depletion in the horizontal magnetic field at stations close to the auroral oval. (This depletion and, thus, the strength of the WEJ, are measured by the geomagnetic AL index). In addition to depleting the horizontal field, the WEJ increases the magnetic field poleward of the auroral oval in the polar cap, where the field is nearly vertical, i.e., almost purely aligned in the Z-direction. Note that the WEJ increases the field in both hemispheres, since in the north (south, respectively) the main field is oriented into (away from) the Earth, and the WEJ produces a downward (upward) oriented field in the northern (southern) polar cap.

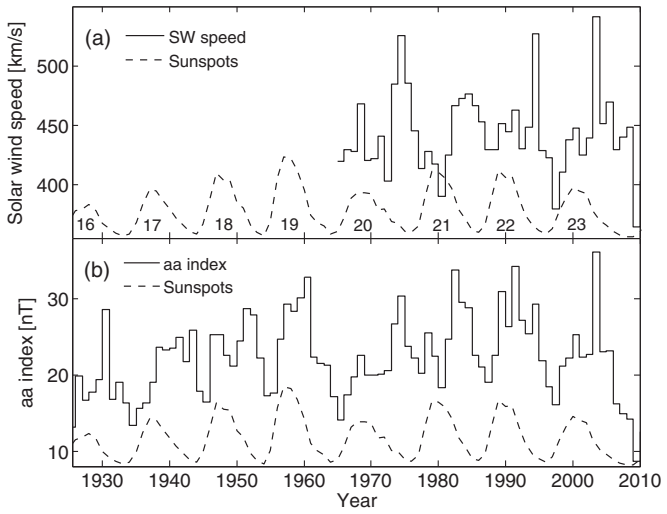

Figure 1. Annual means of solar wind speed and the aa index. (a) Satellite observed solar wind speed in 1965–2010 in units of km s^{-1}. (b) aa index of geomagnetic activity in 1926–2010 in units of nT. Annual sunspot numbers (dashed line without scale) are included as reference in both panels.

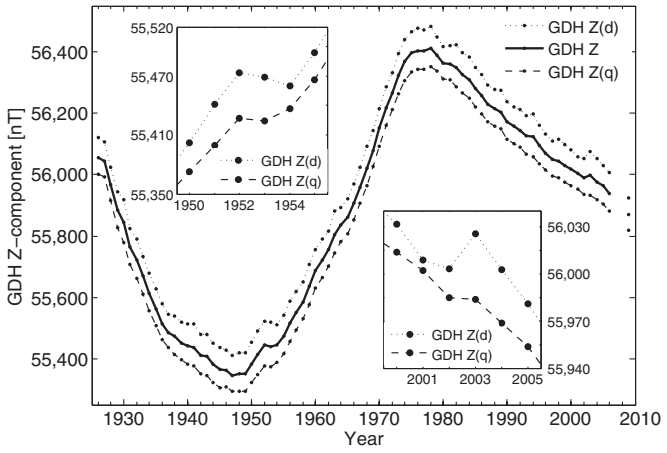

Figure 2. Annual means of the magnetic *Z*-component at the GDH observatory. Annual means of the *Z*-component are depicted separately for all days (*Z*; solid black line), for international quiet days only (*Z*(q); dashed line), and for international disturbed days only (*Z*(d); dotted line) in 1926–2009 in units of nT. Note the data gap in 2007 and 2008. Axis values are valid for the *Z* curve; the dotted curve (dashed curve) has been raised (lowered, respectively) by 50 nT for better visibility. The two inserts depict the annual means for quiet and disturbed days around 1952 and 2003.

2. HSS EFFECT ON THE *Z*-COMPONENT IN THE POLAR CAP

Presenting a new way of studying the solar wind–magnetosphere coupling, it was recently shown (Lukianova et al. 2012) that the annual means of the magnetic field *Z*-component at polar cap observatories are significantly enhanced during the strongest HSS years. Figure 2 depicts the annual means in 1926–2009 (data gap in 2007 and 2008) of the *Z*-component at Godhavn (GDH; 62.25° geographic latitude, 306.47° geographic longitude), the longest running polar cap observatory. In addition to the full year means, Figure 2 also depicts the annual means of the *Z*-component in the magnetically quietest days (called *Z*(q), calculated from the five quietest days of each month), as well in the most disturbed days (called *Z*(d), obtained from the five most disturbed days each month). (In 1932–2009 the internationally selected five quietest and five most disturbed days of each month are based on the geomagnetic Kp index, which exists from 1932 onward. For the earlier years 1926–1931

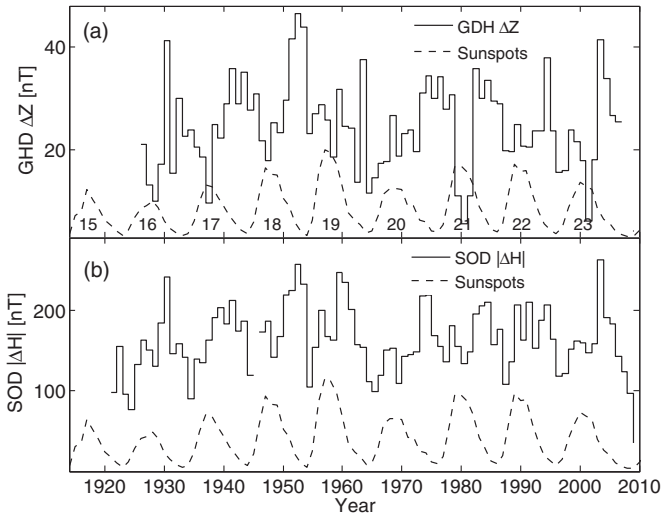

Figure 3. Annual means of GDH ΔZ and SOD $|\Delta H|$. (a) Differences ΔZ of the GDH *Z*-component since 1926 in units of nT. (b) Differences $|\Delta H|$ in the SOD *H*-component since 1914 in units of nT. Annual sunspot numbers (dashed line without scale) are included as reference in both panels.

we have used these days based on the Ci index. Magnetic data were received from the World Data Center at Edinburgh (http://www.wdc.bgs.ac.uk) and SW data were from NASA/NSSDC OMNI2 database (http://omniweb.gsfc.nasa.gov.)

The long-term (secular) evolution of the *Z*-component at GDH during the time depicted in Figure 2 is roughly sinusoidal with amplitude of about one percent of the field intensity. On top of the secular variation Figure 2 shows, particularly clearly in the *Z*(d) curve, several positive deflections, i.e., years of enhanced vertical magnetic field intensity. The two largest positive deflections occurred in 1952 and 2003, and some others, e.g., in 1930, 1941, 1963, 1982, and 1994. It was shown recently (Lukianova et al. 2012), using a number of observatories from both the northern and southern polar cap, that the deflections in the *Z*-component occurred at all stations in the same years, when high-speed stream occurrence and substorm activity (and the related AL index) were at maximum. Accordingly, the *Z*-component of a polar cap station can be reliably used to identify years of persistent HSS activity. The two small inserts in Figure 2 depict an enlarged view of the *Z*(d) and *Z*(q) curves around 1952 and 2003, the two years of the largest deflections. The quiet-day curve *Z*(q) is also somewhat increased in these years, indicating that the persistent high-speed streams raised the *Z*-component even during the quietest days above its normal level. In order to quantify the effect of high-speed streams on the *Z*-component, we remove the quiet time field *Z*(q) from the disturbed time field *Z*(d), constructing annual differences $\Delta Z = Z(\mathrm{d}) - Z(\mathrm{q})$. This difference also removes the seasonal and secular variations of the absolute level of the magnetic field, which is necessary in view of the rather large related variations of the magnetic baseline.

3. ANNUAL SOLAR WIND SPEED FROM δZ

Figure 3(a) depicts the annual means of ΔZ for GDH in 1926–2009. The cycle maxima of ΔZ are found in the declining phase of all the included eight SCs, in agreement with the above discussed SC occurrence of equatorial extensions of coronal holes and high-speed streams at Earth's orbit. In fact, ΔZ has cycle maxima in the same years as SW speed (see Figure 1(a)) for all other cycles except for cycle 21, where SW speed attained closely similar values in a few consecutive years (1982–1985).

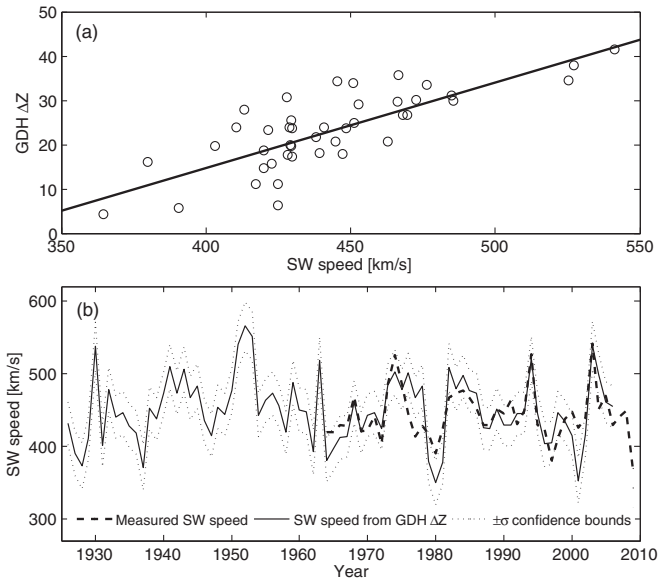

Figure 4. (a) GDH ΔZ plotted as a function of annual averages of solar wind speed. (b) Annual averages of solar wind speed estimated from the GDH ΔZ (solid line) together with their 1σ errors (two dotted lines), and observed annual averages of solar wind speed (thick dashed line).

Accordingly, the annual means of GDH ΔZ and the SW speed must be highly correlated. (Figure 3(b) will be discussed later in Section 5.)

The scatter plot between the annual values of GDH ΔZ and the SW speed is depicted in Figure 4(a). (We note that it is more correct to present ΔZ in terms of SW speed, since SW speed is the driver of ΔZ and known very accurately while ΔZ is known much less accurately. However, practically, the order of correlation makes little difference to the main results.) The correlation coefficient between the annual means of GDH ΔZ and SW speed is $r = 0.78$ which, for 43 annual data points, yields the zero correlation probability of $p = 5.6 \times 10^{-5}$ using Student's t-test and an autoregressive (AR-1) noise model. Thus, SW speed describes the long-term evolution of GDH ΔZ during the last four cycles quite well, explaining 60% ($r^2 = 0.60$) of its inter-annual variation. (Thus, the other possible factors, in particular the IMF strength and orientation, have considerably less influence on GDH ΔZ). Note that the three years (1974, 1994, 2003) of the highest speeds in cycles 20, 21, and 23 stand out in Figure 4(a) as the only years when the annual mean speed is larger than 500 km s^{-1}. Note also that the correlation is fairly linear, indicating applicability over the whole range of ΔZ and SW speed values. (In fact, using a separate fit for high-speed years with, e.g., $V > 450$ km s^{-1} would not lead to greatly different results).

The corresponding annual SW speed values in 1926–2009 (except for 2007 and 2008) estimated from this correlation are shown in Figure 4(b), together with the observed SW speed values in 1965–2009. We have also included there the 1σ (68%) errors for the SW proxies estimated in the following way. We first calculated the standard deviation δ_Z of the residuals of the best fit solution depicted in Figure 4(a). Then we generated a new ΔZ series by adding a random error (following Gaussian distribution with zero mean and standard deviation δ_Z) to each annual ΔZ value, and calculated the SW speed proxy for this series in the same way as for the original ΔZ series. This was repeated 10,000 times, producing a distribution of annual values for each year, whose standard deviations were used as errors for the respective years.

One can see in Figure 4(b) that, overall, the GDH ΔZ values yield a very good proxy for the SW speed at annual resolution for the whole 45 yr time interval. As already seen in Figure 4(a), the proxy covers the range of SW speed values very well, reaching the highest peaks and the lowest minima of SW speed. There are very few years when the proxy deviates from the measured SW speed value by more than one standard deviation. This occurs more systematically only in the ascending phase of cycle 21 (in 1977–1979), when the estimated speed is too large, and during the maximum years of cycles 21 and 23, when the estimates are low.

The annual SW speeds estimated from GDH ΔZ values (see Figure 4(b)) almost double the time of the directly measured SW, covering the whole period of high sunspot cycles of the GMM. Figure 4(b) shows the same long-term evolution as Figure 3(a), now quantified as SW speed. Even if the estimated errors are rather large (due to neglect of other, less important drivers and CMEs), one can find significant differences between the individual years and SCs during the early part of the time series, i.e., during the rising phase of the GMM. Figure 4(b) shows high SW speeds during three years of the declining phase of cycle 18, with maximum speeds in 1952. Accordingly, we find here that the year 1952 was the most HSS active year during the whole GMM.

The annual SW speeds during cycle 17 remained at a rather similar, moderate level over a few consecutive years, thus resembling the situation during cycle 22. However, during cycles 16 and 19 there was one year each (1930 and 1963, respectively) with considerably higher HSS activity than in any other year of those cycles. This is reminiscent of the situation during most of the recent cycles (cycles 20, 22, and 23), where high HSS activity was limited to 1 yr only. Note also that, overall, the HSS activity remained at a rather moderate level during cycle 19, even though this cycle was exceptional in sunspot activity. Cycle 19 was very active in the aa index, too (see Figure 1(b)), which attained larger values during this cycle (with maximum in 1960) than in the earlier cycles. The high peak of the aa index in cycle 19 must therefore be mainly produced by CMEs, whose amount increases with increasing sunspot activity during the rise of the GMM. This comparison demonstrates the different effects of the two SW structures, with HSSs dominating the high-latitude GDH ΔZ and CMEs the mid-latitude aa index (see also Holappa et al. 2014).

4. LOCAL TIME DISTRIBUTION AND SECULAR CHANGE OF ΔZ

It is interesting to study how the auroral electrojets are seen in the mean daily distribution of ΔZ values and how the current systems evolve in time over the GMM period. Figure 5 shows the annual averages of ΔZ in color scale, separately for each hour of the day (vertical axis) and each year (horizontal axis). Each narrow vertical color strip then presents the yearly averaged LT distribution of ΔZ. Positive values (yellow to red in the color code of Figure 5) depict the average LT location of the WEJ and negative values (blue to black color) that of the eastward electrojet (EEJ). One can see in Figure 5 that the WEJ region is centered around the local midnight to post-midnight hours and the EEJ in the local noon to afternoon sector. The WEJ region is wider in LT, about 12 hr on average, while the typical extent of the EEJ region is about 8 hr. Therefore, e.g., the total annual ΔZ values (used above), which are averages of the 24 hourly values depicted in Figure 5, are all positive.

Figure 5 shows that, in certain years, the WEJ extends over a wider LT range than average. This is particularly clearly

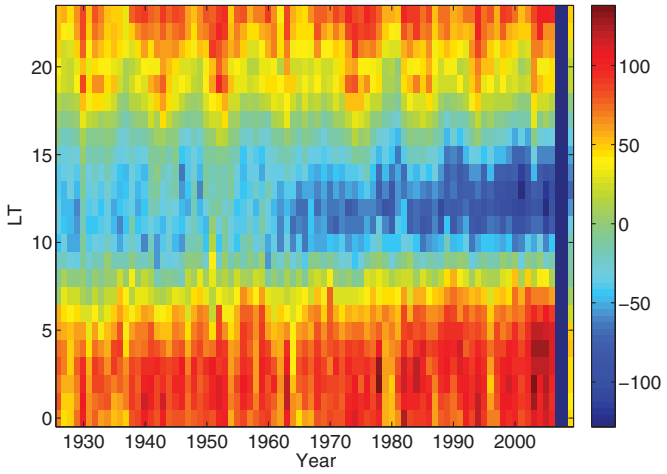

Figure 5. Annual means of GDH ΔZ in color coding for each local time hour (vertical axis) and year (horizontal axis). For each year the annual mean of GDH ΔZ is separately calculated for each of the 24 hr of local time. Color axis gives the scale of ΔZ values in units of nT.

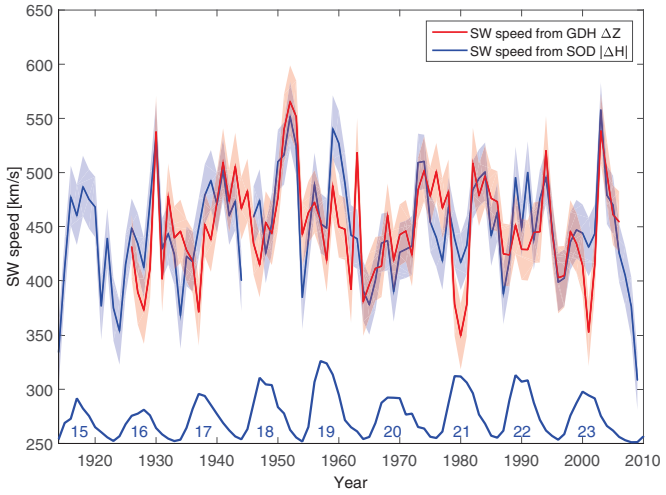

Figure 6. Annual means of solar wind speed extracted from GDH ΔZ (red lines) and SOD $|\Delta H|$ (blue lines) with respective 1σ errors in units of km s^{-1} denoted as shaded areas. Annual sunspot numbers (blue line without scale) are included as a reference.

seen as the extension of the WEJ region from the midnight (top of Figure 5) toward the evening sector (downward in Figure 5). (A corresponding extension also takes place in the morning, but generally remains less notable). As seen in Figure 5 large extensions occur roughly once every SC and, in fact, correspond exactly to the years of the most persistent HSS activity discussed above. For example, in the early 1950s the WEJ region extends from midnight until about 16 LT, reducing the average intensity and extent of the EEJ in these years. The extension of the WEJ from midnight toward afternoon is related to the dynamics of the magnetosphere during substorms (in particular to the development of the westward traveling surge; see, e.g., Lockwood 2013) whose occurrence is maximized during HSS years (Tanskanen et al. 2005, 2009). Accordingly, the connection between high-speed streams and WEJ extensions is well understood.

Figure 5 also indirectly depicts the effect of the secular change of the geomagnetic field upon the auroral electrojets, as observed at the GDH station. Secular change moves the geomagnetic latitude of the GDH station roughly by 1.6° southward and, thereby, closer to the auroral oval, from the 1940s until the present. This slow change artificially intensifies the auroral electrojets observed at GDH, as depicted by the systematic intensification of colors (positive and negative values of ΔZ) in Figure 5. However, since this secular evolution enhances both the westward and the EEJ observed at GDH roughly equally, it has no significant effect on SW speeds extracted from the annual means of GDH ΔZ values, which are the means of the 24 LT values depicted in Figure 5.

5. HSS EFFECT ON THE *H*-COMPONENT AT SUB-AURORAL LATITUDES

Although the effect of HSSs is more purely observed on the polar side of the auroral oval, we have studied the long-term evolution of the WEJ intensity also using the horizontal (H) component of the Sodankylä station (SOD, 67.37° geographic latitude, 26.63° geographic longitude), which is located equatorward from the auroral oval (at a sub-auroral latitude) and has one of the longest contiguous measurements since 1914. Contrary to GDH, the magnetic activity at the sub-auroral SOD station is not only affected by the HSSs, but also by the storms and strong substorms due to CMEs, which expand the auroral oval equatorward more than the HSS-related weaker substorms (Holappa et al. 2014). (Note that we cannot use the Z-component to study the WEJ at sub-auroral latitudes).

In order to reduce the effect of CMEs at SOD, we have used SOD observations only around the local midnight, where the WEJ has its maximum (see Figure 5) and where the connection to SW speed is most direct (Finch et al. 2008). Figure 3(b) shows the annual means of $|\Delta H|$ (note that $\Delta H = H(\mathrm{d}) - H(\mathrm{q})$ is negative) at SOD in the 22–02 LT sector. (For the earliest years, 1914–1925, of the SOD station we have used the station's own K indices to determine the quietest and most disturbed days.) SOD $|\Delta H|$ values depict considerable similarity with the long-term evolution of GDH ΔZ values. In particular, they verify that HSS activity had its long-term maximum in 1952, during the declining phase of cycle 18. Note that both GDH ΔZ and SOD $|\Delta H|$ values deviate from the long-term evolution of the mid-latitude aa index (Figure 1(b)). The differences between GDH ΔZ and SOD $|\Delta H|$ are due to CMEs, which raise SOD $|\Delta H|$ activity in solar maximum years, especially around 1960 and 1990, above the level caused by HSSs (that are more reliably represented by GDH ΔZ values).

Despite the effect of CMEs, the annual means of SOD $|\Delta H|$ and SW speed are also highly correlated, and have a correlation coefficient of 0.79 which, for 45 annual data points, yields the zero correlation probability of $p = 1.2 \times 10^{-5}$. The annual SW speeds derived from SOD $|\Delta H|$, together with the speeds obtained from GDH ΔZ (copied from Figure 4(b)) are shown in Figure 6. The error bars for speeds obtained from SOD $|\Delta H|$ were calculated in the same way as for GDH ΔZ. Figure 6 shows that SOD $|\Delta H|$ values give higher speeds around the sunspot maxima of cycles 19 and 22, and raise the low level around the maximum of cycle 21 higher. They also yield a somewhat higher peak in 2003. These differences are, as noted above, mainly due to the effect of CMEs, which have a larger effect on the $|\Delta H|$ values of the sub-auroral SOD station than on the GDH ΔZ. Therefore, the results based on the GDH ΔZ more truthfully represent the long-term evolution of HSS activity than those based on the SOD $|\Delta H|$. Despite these differences, there is good overall agreement between the results extracted from the two stations at opposite sides of the auroral electrojet. In particular, both stations agree on the uniqueness of HSS activity in cycle 18, and that the year 1952 was the year of maximum

HSS activity over the whole GMM. Note that this agreement excludes the possibility that secular evolution would seriously modify the long-term consistency of GDH observations.

6. DISCUSSION AND CONCLUSIONS

We have used here a recently presented method based on the Z-component of the magnetic field at a polar cap station (Lukianova et al. 2012) to study the occurrence of high-speed SW streams. Using the observations of the longest recording polar cap (GDH) station, we have estimated the annual mean SW speeds over the GMM from 1920s onward. Since the Z-component of a polar cap station closely responds to HSSs, the method gives the annual mean speeds of the HSSs occurring during the year. As the high-speed streams have a roughly constant speed (about 800 km s^{-1}), the annual mean speeds determined in this way reflect the relative occurrence of these streams at Earth's orbit.

We find that persistent HSS activity occurred in the declining phase of all eight SCs studied. During five of the eight cycles (cycles 16, 19, 20, 22, 23) one year clearly stood out as the year with the maximum HSSs in the respective cycle. During two other cycles (cycles 17 and 21), HSS activity was distributed over a number of consecutive years, whose HSS activity always remained below the typical level of the single-year maxima. These results can be understood in terms of a typical evolution of coronal hole extension (solar dipole tilt activation, sometimes also called the solar excursion phase). Such an extension dies out completely during some seven to eight rotations (Mursula & Zieger 1996), weakening its amplitude during this time and having an effective HSS occurrence time of about five rotations. This structure occurs randomly in time, hence the probability of having the whole extension period within one calendar year is about 2/3, in fair agreement with the above fraction of 5/8. (Of course, a more refined treatment also needs to take the uneven seasonal distribution of HSSs into account).

We find that the most persistent HSS activity occurred in the early 1950s, in the declining phase of SC 18. High HSS activity continued for three successive years, with the highest activity found in the year 1952. Considering the above statistics of HSS occurrence during the other cycles of the GMM, this period (the declining phase of cycle 18) is exceptional. According to solar dynamo theory, the strength of the solar polar magnetic fields during a sunspot minimum determines the level of sunspot activity during the next solar maximum (Babcock 1961; Leighton 1964, 1969; Charbonneau 2005). However, this basic tenet of solar magnetism has remained unverified even for GMM, the highest activity of measured sunspot history, because of the lack of direct observations of solar polar fields.

The same activations of new solar flux at the mid-latitudes that lead to the polar coronal hole extensions (solar excursion phases) also enhance the intensity of the recently changed new-polarity field at the poles via the poleward meridional flow of the trailing flux. Therefore, the more frequent and stronger the activations in the declining phase, the longer the HSSs occur at low latitudes and the stronger the solar polar fields will get. Therefore, there is indeed a connection between the annual occurrence frequency of HSSs at Earth's orbit in the declining phase of the SC and the intensity of the solar polar fields during the subsequent minimum. In view of this connection, our finding of exceptional high-speed stream activity in the declining phase of SC 18 suggests that cycle 19 was indeed preceded by exceptionally strong polar fields during the previous sunspot minimum, thus giving interesting support for the validity of solar dynamo theory during this dramatic period of solar magnetism.

Finally, we note that some earlier studies have indicated fairly strong but no exceptional SW speeds in 1952 (Svalgaard & Cliver 2007; Rouillard et al. 2007; Lockwood et al. 2009; Lockwood et al. 2014). Typically these studies use various combinations of GA at mid-latitudes (like the aa index in Figure 1(b)), where the effect of CMEs is relatively larger than at auroral latitudes, especially during solar maximum years. Finding out the detailed causes of the differences between these and the present results will, however, have to be postponed to a separate study. Note that Lockwood & Owens (2014) have proposed a model whereby the observed centennial variation in the annually averaged SW speed is connected to the changes in the width of the streamer belt. While completely different in its approach, this model is conceptually in a very good agreement with the present results, excluding the detailed differences for SW speed in individual years, as discussed above. We also note that, recently, a long-term proxy was developed for the hemispheric polar field strengths since 1905 using polar faculae, calibrated to the polar flux observations during the last decades (Muñoz-Jaramillo et al. 2013). They found the largest value in the northern hemisphere during cycle 18, partly supporting the present observations.

We thank all providers of the data used in this work, including the OMNI and the WDC databases. We acknowledge the financial support by the Academy of Finland to the ReSoLVE Center of Excellence (project No. 272157) and to project Nos. 140329 and 140403. We also acknowledge the support for this work by uniOGS of the University of Oulu and by the COST Action ES1005 "TOSCA" (http://www.tosca-cost.eu).

REFERENCES

Abreu, J. A., Beer, J., Steinhilber, F., Tobias, S. M., & Weiss, N. O. 2008, GeoRL, 35, 20109
Babcock, H. W. 1961, ApJ, 133, 572
Bame, S. J., Asbridge, J. R., Feldman, W. C., & Gosling, J. T. 1976, ApJ, 207, 977
Charbonneau, P. 2005, LRSP, 2, 2, http://www.livingreviews.org/lrsp-2005-2
Finch, I. D., Lockwood, M. L., & Rouillard, A. P. 2008, GeoRL, 35, 21105
Holappa, L., Mursula, K., Asikainen, T., & Richardson, I. G. 2014, JGR, 119, 4544
Kojima, M., & Kakinuma, T. 1990, SSRv, 53, 173
Krieger, A. S., Timothy, A. F., & Roelof, E. C. 1973, SoPh, 29, 505
Lefèvre, L., & Clette, F. 2011, A&A, 536, L11
Leighton, R. B. 1964, ApJ, 140, 1547
Leighton, R. B. 1969, ApJ, 156, 1
Livingston, W., & Penn, M. 2009, EOS Transactions, 90, 257
Lockwood, M. 2013, LRSP, 10, 4
Lockwood, M., Nevanlinna, H., Barnard, L., et al. 2014, AnGeo, 32, 383
Lockwood, M., & Owens, M. J. 2014, ApJL, 781, L7
Lockwood, M., Rouillard, A. P., & Finch, I. D. 2009, ApJ, 700, 937
Lukianova, R., Mursula, K., & Kozlovsky, A. 2012, GeoRL, 39, 4101
Mayaud, P.-N. 1972, JGR, 77, 6870
Muñoz-Jaramillo, A., Dasi-Espuig, M., Balmaceda, L. A., & DeLuca, E. E. 2013, ApJL, 767, L25
Mursula, K., & Zieger, B. 1996, JGR, 101, 27077
Penn, M. J., & Livingston, W. 2006, ApJL, 649, L45
Richardson, I. G., Cane, H. V., & Cliver, E. W. 2002, JGR, 107, 1187
Rickett, B. J., & Coles, W. A. 1991, JGR, 96, 1717
Rouillard, A. P., Lockwood, M., & Finch, I. 2007, JGR, 112, A05103
Solanki, S. K., Usoskin, I. G., Kromer, B., Schüssler, M., & Beer, J. 2004, Natur, 431, 1084
Svalgaard, L., & Cliver, E. W. 2007, JGR, 112, 10111
Tanskanen, E. I., Pulkkinen, T. I., Viljanen, A., et al. 2011, JGR, 116, A00I34
Tanskanen, E. I., Slavin, J. A., Tanskanen, A. J., et al. 2005, GeoRL, 32, 16104